Rapid Communications

Quantitative analysis of the electronic decoupling of an organic semiconductor molecule at a metal interface by a monolayer of hexagonal boron nitride

Christine Brülke,[1] Timo Heepenstrick,[1] Ina Krieger,[1] Beatrice Wolff,[1] Xiaosheng Yang,[2,3] Ali Shamsaddinlou,[2,3] Simon Weiß,[2,3] François C. Bocquet,[2,3] F. Stefan Tautz,[2,3] Serguei Soubatch,[2,3] and Moritz Sokolowski[1]

[1]*Institut für Physikalische und Theoretische Chemie, Universität Bonn, Wegelerstrasse 12, 53115 Bonn, Germany*

[2]*Forschungszentrum Jülich, Peter Grünberg Institut (PGI-3), 52425 Jülich, Germany*

[3]*Jülich Aachen Research Alliance (JARA), Fundamentals of Future Information Technology, 52425 Jülich, Germany*

(Received 29 March 2018; revised manuscript received 29 January 2019; published 11 March 2019)

The adsorption geometry, the electronic properties, and the adsorption energy of the prototype organic molecule 3,4,9,10-perylene tetracarboxylic dianhydride (PTCDA) on a monolayer of hexagonal boron nitride (hBN) grown on the Cu(111) surface were determined experimentally. The perylene core is at a large height of 3.37 Å and only a minute downward displacement of the functional anhydride groups (0.07 Å) occurs, yielding adsorption heights that agree with the sum of the involved van der Waals radii. Thus, already a single hBN layer leads to a decoupled (physisorbed) molecule, contrary to the situation on the bare Cu(111) surface.

DOI: 10.1103/PhysRevB.99.121404

Wide band gap two-dimensional materials (2DMs) [1,2], as, for instance, hexagonal boron nitride (hBN), are of interest as interfacial layers for separating the electronic states of adjacent conducting or semiconducting materials [3]. The appeal of hBN is given by the possibility to grow hBN mono- and multilayers [4] on many metallic substrates by chemical vapor deposition of borazine [5–7]. The hBN layer of monoatomic thickness is particularly interesting as it represents the ultimate case of a thin interfacial barrier. In short, the hBN monolayer constitutes a π bonded honeycomb net with alternating boron and nitrogen atoms [8]. It is known that multilayer sheets of hBN constitute a good electrical insulator with a wide band gap [9]. But how do these properties scale down to the single hBN monolayer and how well does this still separate the electronic states located at its two interfaces? This aspect appears to be important for the understanding and optimization of electronic thin film devices based on monoatomic hBN layers or similar other 2DMs in general. Obviously, an experimental clarification requires monitoring the electronic properties on the hBN layer at the microscopic level. One approach is to use the adsorption of an organic molecule as a probe. Investigations of this kind have been made by comparing the submolecular contrast in scanning tunneling microscopy (STM) images to that expected for the unperturbed molecular orbitals [10,11]. Here, we go further and measure the electronic *and* structural response of an organic molecule on an hBN/metal surface. Furthermore, we quantify the remaining interfacial bonding by the adsorption energy.

The Cu(111) surface lends itself to this purpose because, for building devices, hBN layers are commonly grown on Cu foils [12,13]. In a preceding experiment we have already determined the distance of the hBN layer to the underlying topmost Cu(111) layer [14]. The large value of 3.24 Å exceeds the sum of the van der Waals (vdW) radii of the interfacial atoms significantly [$(r_{\mathrm{N}}^{\mathrm{vdW}} + r_{\mathrm{Cu}}^{\mathrm{vdW}}) = 2.86$ Å and $(r_{\mathrm{B}}^{\mathrm{vdW}} + r_{\mathrm{Cu}}^{\mathrm{vdW}}) = 3.05$ Å] and identifies the bonding between the hBN layer and the Cu(111) surface as very weak. The analysis also revealed no signs of a vertical long-range modulation of the hBN layer caused by its misfit to the Cu(111) surface [14]. We therefore consider it as perfectly flat in the following. As a consequence of the large interfacial hBN/Cu(111) distance and its band gap of 5–6 eV [15], the probability density of metal states should be strongly reduced at the hBN/vacuum interface. In conclusion, a molecule placed onto this surface should show negligible features for electronic and structural modifications due to interactions of molecular and metallic states, and thus its properties should be very close to those expected for a *physisorbed* molecule. However, quantitative information is desirable here, not at least because recent observations point in different directions: On the one hand, an electronic corrugation due to the misfit to the Cu(111) substrate is present on the hBN/Cu(111) surface [16] and reveals itself by a template effect on the adsorption of molecules [11,17–19]. Furthermore, a "catalytic transparency" of hBN on Cu(111) has been stated [20,21], which indicates a "leaking" of the metal states through the hBN that enables borazine dissociation on a closed hBN layer. On the other hand, STM images show small perturbations of the molecular states on the hBN/Cu(111) surface indicating efficient decoupling [17].

We use the semiconductor model molecule 3,4,9,10-perylene tetracarboxylic dianhydride [PTCDA, cf. Fig. 1(d)] in order to take advantage of the fact that the structural and electronic details of adsorbed PTCDA molecules have been documented for a wide range of different metal surfaces [22–25]. The height of the perylene core above the surface is dependent on the substrate due to varying strengths in bonding and interactions with metallic states, as seen by the energetic shifts of the PTCDA valence orbitals [26–29]. In addition, characteristic vertical displacements of the functional anhydride groups out of the molecular plane of the otherwise planar molecule occur. The pattern and size of these structural distortions bear information about the bonding of the molecule to the surface. For example, on the bare Cu(111) surface, the distortion of the anhydride groups encompasses

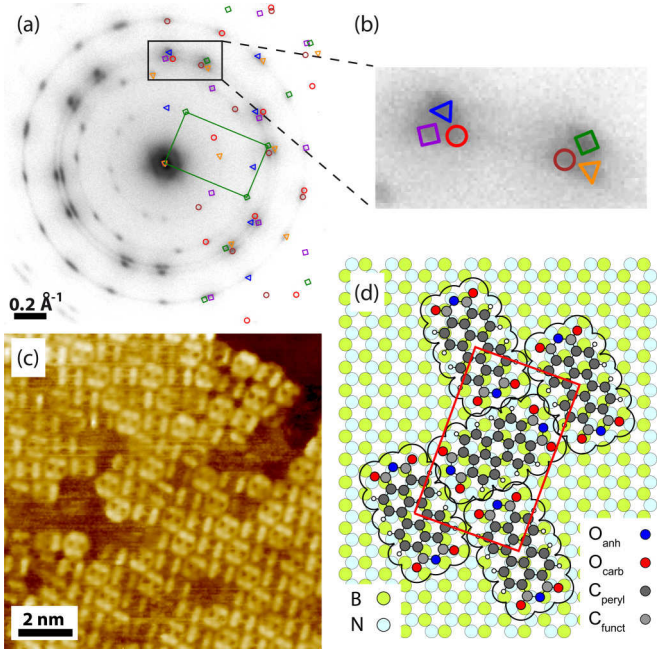

FIG. 1. (a) Overview LEED pattern of one monolayer PTCDA on hBN/Cu(111) with superimposed calculated spot positions and reciprocal unit cell (green). Different colors refer to six symmetry equivalent domains. The pattern was recorded at an electron energy of 30.4 eV and a sample temperature T of 110 K. (b) Zoom-in of the detail marked in (a). (c) STM image of PTCDA molecules on hBN/Cu(111) arranged in a herringbone pattern. The image was recorded at $U_{bias} = +1.5$ V and $I = 500$ pA at $T = 300$ K. (d) Corresponding hard-sphere model of the unit cell. The covalent atom radii in the molecules are drawn at 75% of their sizes for clarity. The envelope of the vdW spheres and the unit cell of the PTCDA lattice (red) are indicated.

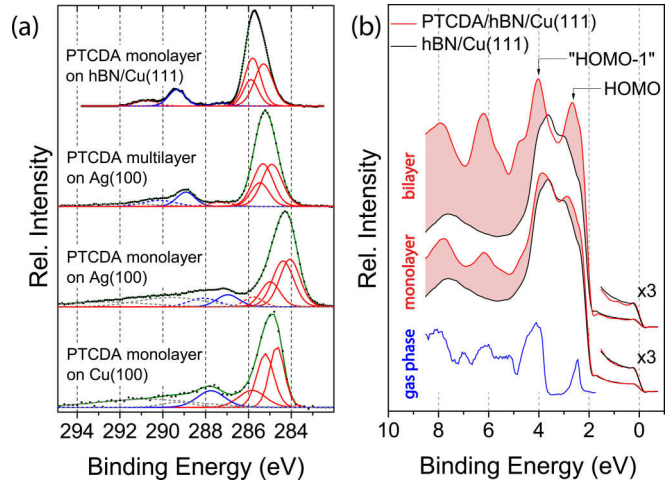

FIG. 2. (a) XPS data for the C 1s level of PTCDA on different surfaces. Contributions from the different C atoms have been fitted and are indicated by different colors; red: different C atoms of the perylene core; blue: functional carbon atoms; dashed: respective satellites; dashed gray: nonassigned satellites. For details of the assignment, see Ref. [23] [Ag(100) spectra taken from Refs. [23,34]; Cu(100) spectrum taken from Ref. [24]]. (b) UPS data of the bare hBN/Cu(111) interface (black curve), and the PTCDA monolayer and bilayer on hBN/Cu(111) (red curves). The spectra are angle integrated over an emission angle between 8° and 25°, and were normalized by the height of the Fermi edge. A zoom of the Fermi edge is shown. Spectra were measured using He IIα radiation in 45° incidence. For comparison, a gas phase spectrum of PTCDA is shown (blue curve, taken from Ref. [35]; the spectrum was aligned at the HOMO position).

a vertical shift of the central O atom (O_{anh}) by 0.23 Å with respect to the perylene core in the direction away from the surface, while the carboxylic O atoms (O_{carb}) and the functional C atoms (C_{funct}) stay approximately at the height of the perylene core (C_{peryl}). [See Fig. 1(d) for the nomenclature.] This indicates a chemical interaction that is dominantly located on the perylene core [25]. Here, we use these effects as a delicate probe to test the coupling of leaking Cu states at the hBN/vacuum interface with molecular orbitals.

Figure 1 comprises structural data on a PTCDA monolayer adsorbed on the hBN/Cu(111) heterostructure. The low-energy electron diffraction (LEED) image reveals the formation of ordered domains. The PTCDA lattice is found to be incommensurate with respect to the hBN lattice. The lattice parameters can be identified from the spot positions in the LEED image with high precision, as it was done, e.g., for PTCDA on the Ag(111) surface before [30]. They were determined with an accuracy of 0.5% and agree within 3% with those of PTCDA layers in the β modification of the bulk crystal [31]. The achieved fit of calculated and measured LEED spot positions is shown in the zoom-in displayed in Fig. 1(b). Notably, the spots are not sharp, but smeared out azimuthally. This is due to the imperfect azimuthal order of the hBN domains [14] that is imprinted on the PTCDA layer. The STM image [Fig. 1(c)] gives further insight into the structure: There are two molecules per unit cell forming the well-known herringbone arrangement stabilized by hydrogen bonds [Fig. 1(d)] that is seen for PTCDA on many surfaces [32]. But STM also reveals a high density of domain boundaries involving the azimuthal rotation of individual or groups of molecules. STM imaging was only successful for tunneling into unoccupied states and the obtained submolecular contrast resembles the lowest unoccupied orbital (LUMO) [33]. The observed incommensurate structure and the bulklike lateral packing point to a very weak interaction of PTCDA with hBN, leading to an only small lateral corrugation of the interaction potential. However, the possibility to draw a tunnel current from the PTCDA layer indicates that some, at least very weak, coupling to metallic states must still exist here.

Figure 2(a) displays C 1s x-ray photoelectron spectroscopy (XPS) data taken for PTCDA on hBN/Cu(111) in comparison to spectra for a multilayer and for PTCDA monolayers on the bare Cu(100) and Ag(100) surfaces. The important observation from these spectra concerns the energetic shift of the peak related to the four C_{funct} atoms with respect to the position of the main peak stemming from the 20 central C_{peryl} atoms. While on hBN and for the PTCDA multilayers the C_{funct} peak is located at a binding energy 4 eV below the C_{peryl} peak, it is shifted by 1.5 eV towards the latter on the metal surfaces. This differential shift marks the chemical bonding of the PTCDA to the metal surfaces and has been discussed in detail [26].

Concurrently, the very good agreement of PTCDA/hBN and the multilayer spectra identifies the bonding situation on hBN as similar to that between PTCDA multilayers.

Commonly, the coupling of PTCDA to metallic states leads to shifts in the frontier orbitals [26,27]. A significant downward shift of the LUMO to or even below the Fermi energy and small upward shifts of the HOMO (highest occupied orbital) and the "HOMO-1 band" (which consists of four individual orbitals [36]) are typical [26]. Quite differently, at the hBN/Cu(111) surface, the energetic distances between the frontier orbitals are not altered with respect to those seen for gas phase spectra. This is illustrated by the ultraviolet photoemission spectra (UPS) displayed in Fig. 2(b). The binding energies and partially also the relative intensities of the well-resolved HOMO and the unresolved groups of lower-lying orbitals of the gas phase spectrum [35] are well reproduced in both the spectra of a PTCDA mono- and bilayer on hBN. On bare Cu(111), the LUMO is filled due to hybridization with Cu states and found at a binding energy of 0.8 eV [27]. In contrast, for hBN/Cu(111), we see a continuous intensity related to metal states ($E_{\mathrm{Bind}} \leqslant 2$ eV) with no indications for a contribution of a former LUMO which excludes any charge transfer from the metal to the molecule. Work-function changes derived from the cutoffs in UPS data compliment the finding of an absent metal-molecule coupling: A negative change of the work function ($\Delta\Phi = -0.5$ eV) upon deposition of the hBN layer on the Cu(111) surface shows that hBN suppresses the spill-out of the Cu states. Upon PTCDA deposition on hBN/Cu(111), we find *no* significant further reduction of the work function (-0.05 eV $< \Delta\Phi < 0$ eV) caused by a possible pushback of the metallic states, which is typically encountered for PTCDA adsorption on metal surfaces [27]. This is compatible with a low probability density of Cu states at the PTCDA/hBN interface. In summary, we deduce the following: A PTCDA monolayer on hBN displays the structural and electronic signatures which are expected for a *physisorbed* molecule. Thus, the final question is whether this conclusion can be corroborated by the structural parameters of the adsorption complex.

To this end, we have determined the vertical heights of chemically and thus electron spectroscopically discernible atoms with respect to the hBN layer by the normal incidence x-ray standing wave (NIXSW) technique [40]. The data analysis was performed by the program TORRICELLI [41] and included necessary nondipolar corrections (cf. Ref. [14]). Table I summarizes the results. The underlying electron yield curves, respective fits, and the corresponding Argand diagram are shown in Fig. 3. The vertical position of the hBN layer covered by PTCDA was also determined in this experiment by NIXSW in the same manner as reported earlier for the bare hBN/Cu(111) heterostructure [14]. The obtained positions were identical within the error in both experiments, which means that PTCDA does not change the height of hBN. The theoretical fits to the experimental NIXSW curves of PTCDA are good, and the coherent fractions, which are between 0.60 and 0.85, are in agreement with our expectation based on results from other similar NIXSW experiments [22–25].

For the perylene core we find a vertical height of $d_{\mathrm{c}}^{\mathrm{hBN}}(\mathrm{C_{peryl}}) = 3.37$ Å above the hBN layer. This is the largest adsorption height which has been reported so far for the perylene core of PTCDA on any surface [22–25,42]. This distance is well fitted by the sum of the vdW spheres of B and C ($r_{\mathrm{B}}^{\mathrm{vdW}} = 1.65$ Å, $r_{\mathrm{C}}^{\mathrm{vdW}} = 1.75$ Å [39]). We refer to B, and not to N, to describe the hBN surface, because B exhibits a slightly larger vdW radius and because B is

TABLE I. Coherent fractions f_{c} (describing the height distribution) and coherent positions p_{c} of four chemically inequivalent atoms of the PTCDA molecule and derived respective vertical distances $d_{\mathrm{c}}^{\mathrm{Cu}}$ and $d_{\mathrm{c}}^{\mathrm{hBN}}$ with respect to the topmost Cu(111) and hBN layer, respectively. $d_{\mathrm{c}}^{\mathrm{Cu}}$ and $d_{\mathrm{c}}^{\mathrm{hBN}}$ were calculated as $d_{\mathrm{c}}^{\mathrm{Cu}} = (n + p_{\mathrm{c}}) \cdot d_{(111)}^{\mathrm{Cu}}$ and $d_{\mathrm{c}}^{\mathrm{hBN}} = d_{\mathrm{c}}^{\mathrm{Cu}} - d^{\mathrm{hBN}}$, with $n = 3$, $d_{(111)}^{\mathrm{Cu}} = 2.087$ Å [37], and $d^{\mathrm{hBN}} = 3.24(3)$ Å [14]. $n = 3$ is derived because other values give unreasonable distances.

	f_{c}	p_{c}	$d_{\mathrm{c}}^{\mathrm{Cu}}$ (Å)	$d_{\mathrm{c}}^{\mathrm{hBN}}$ (Å)
$\mathrm{O_{carb}}$	0.59(1)	0.128(3)	6.528(6)	3.29(3)
$\mathrm{O_{anh}}$	0.64(2)	0.135(4)	6.543(8)	3.30(3)
$\mathrm{C_{funct}}$	0.83(5)	0.137(9)	6.547(19)	3.31(4)
$\mathrm{C_{peryl}}$	0.85(2)	0.169(3)	6.614(6)	3.37(3)

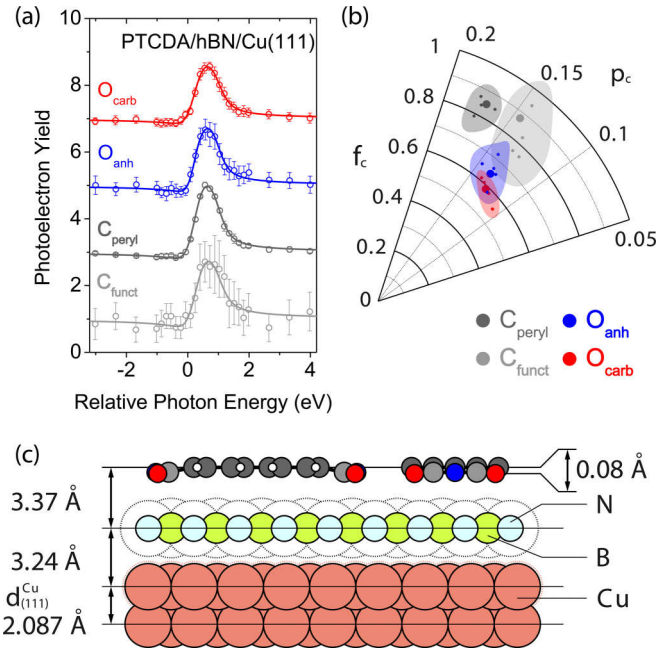

FIG. 3. (a) Electron yield curves from NIXSW data (angle integrated) for $\mathrm{O_{carb}}$, $\mathrm{O_{anh}}$, $\mathrm{C_{funct}}$, and $\mathrm{C_{peryl}}$ (vertically shifted). Photon energies are given relative to the Bragg energy of Cu(111). (b) Argand diagram showing the results of all data sets and the respective averaged values (heavy symbols). Shaded areas mark the envelope of the error bars of the data sets. The O 1*s*/C 1*s* level was evaluated on five/four different positions on the sample. Note that the coherent position of the $\mathrm{C_{peryl}}$ signal is by ~0.03 larger than those of the other three species, which are about the same. (c) Side views of PTCDA/hBN/Cu(111) along the short and long molecular axes. The vertical distances within the PTCDA molecule are enlarged by a factor of 4 and the covalent radii of PTCDA are drawn at 75% of their sizes in order to better show the very small downwards bending of the terminal anhydride groups. For the hBN layer the vdW spheres are indicated.

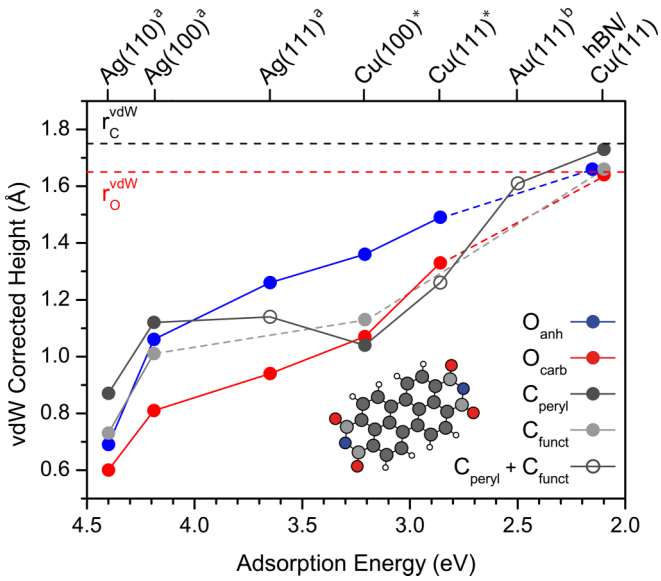

FIG. 4. Adsorption heights of chemically discernible groups in PTCDA on various surfaces as determined by NIXSW [22–25] corrected (i.e., reduced) by the vdW radii of the respective surface atoms vs the adsorption energies E_{ads} (data marked by "a" and "b" taken from Ref. [23] and Ref. [38], respectively). For Cu(100) and Cu(111) (marked by $*$) E_{ads} values are not available and horizontal data point positions are only qualitatively placed according to the work-function trend [24]. The data illustrate the trend of the bonding height from stronger chemisorptive bonding (left) to weak physisorptive bonding (right). The vdW radii were taken from Ref. [39]: $r_{Ag}^{vdW} = 1.72$ Å, $r_{Cu}^{vdW} = 1.40$ Å, $r_{Au}^{vdW} = 1.66$ Å. For the hBN substrate the boron radius was used, because it is larger ($r_B^{vdW} = 1.65$ Å; $r_N^{vdW} = 1.46$ Å) and because B is located by 0.03 Å higher than N [14]. For Ag(111), Cu(111), and Au(111), the positions of C_{peryl} and C_{funct} were not analyzed individually. Thus, averaged values for all C atoms ($C_{peryl} + C_{funct}$) are shown there. For the Au(111) surface the position of the O atoms could not be determined for experimental reasons [22]. The lines linking the data points are guides for the eye. Dashed lines indicate incomplete data. The horizontal dashed lines mark the vdW radii of carbon and oxygen. The value $r_C^{vdW} = 1.75$ Å is valid for sp^2 hybridized carbon in perylene, in the direction perpendicular to the molecular plane [39]. The value $r_O^{vdW} = 1.65$ Å is the average of 1.6 and 1.7 Å, the range covering the generally found radii for sp^2 hybridized oxygen parallel to its double-bond axis [39].

positioned by 0.03 Å higher than N [14]. The agreement with the vdW radii also holds true within error for the atoms in the terminal anhydride groups (O_{carb}, O_{anh}, C_{funct}). We have illustrated this in Fig. 4. There we have also included available data for PTCDA on different metal surfaces for comparison. The bonding heights are given as corrected bonding heights, meaning that we have subtracted the vdW radii of the respective surface atoms. The corrected bonding heights can thus be directly compared to the vdW radii of the respective atoms of PTCDA. We have ordered the metal surfaces from left to right with increasing work functions, which marks to some degree the trend of decreasing strength of the chemisorptive interaction [24]. This order is further justified by the adsorption energies (E_{ads}) given on the x axis where they are available. For the present system we have determined E_{ads} from the desorption energy that was measured by thermal desorption spectroscopy [43–46] as described in the Supplemental Material (SM) [47]. For estimating the contribution of the intermolecular interactions to E_{ads} we used data available for the PTCDA/Ag(100) system [48,49].

The situation on hBN falls on an extreme. For comparison, on the Au(111) surface, for which the bonding is considered physisorptive, a height of the perylene core of 3.27 Å was obtained [22]. The large bonding height of the perylene core on hBN/Cu(111) is remarkable and identifies the interaction of the PTCDA molecule with this surface as extremely weak. It is mirrored by a decrease of E_{ads} to a small value of 2.10 ± 0.09 eV which is by 0.4 eV smaller than that on Au(111) (see SM for details). Indeed, the only indication for the presence of the interface imprinted on the structure of the PTCDA molecule is a very minute downward shift of the peripheral anhydride groups including both types of oxygen atoms O_{carb}, O_{anh} and the functional carbon atoms C_{funct}. The averaged downward shift with respect to the perylene core amounts to 0.07 Å (the largest downward shift is that of O_{carb} by 0.08 Å). The molecule is thus *not* fully planar. However, we interpret this not as a consequence of a chemical interaction. Instead, it must be due to the attractive local vdW interactions of the O atoms with the surface, and/or an electrostatic interaction of the partially negatively charged O atoms with image charges in the Cu substrate. Apparently, the C_{funct} atoms follow the oxygen atoms in their move.

In conclusion, the hBN layer suppresses the Cu wave functions at the hBN/vacuum interface, such that adsorption has little influence on structural and electronic, i.e., the ground state, properties of PTCDA. It remains to be proven in how far this is also true for excited state properties, e.g., lifetimes of electronic excitations. In hindsight the template effect of hBN/Cu(111) on molecular adsorption noted at the beginning must be due to a very small local variation of the adsorption energy that is compatible with a physisorptive bonding.

Note added. Recently, we became aware of two publications that are interesting in the context of the present work. A similar study of a molecule on hBN/Cu(111) was reported [50]; for PTCDA adsorbed on hBN multilayers an adsorption energy of 2.46 eV and a vertical distance of 3.1 Å were found from calculations by density functional theory [51].

Acknowledgments. We thank Diamond Light Source for access to beamline I09 (SI14878) that contributed to the results presented here and the team of the beamline I09, D. Duncan, P. Kumar, and T.-L. Lee. Financial support by the DFG under Project No. So407/6-3 and SFB 1083 is acknowledged.

[1] K. S. Novoselov, A. Mishchenko, A. Carvalho, and A. H. Castro Neto, 2D materials and van der Waals heterostructures, Science **353**, 461 (2016).

[2] A. C. Ferrari, F. Bonaccorso, V. Fal'ko, K. S. Novoselov, S. Roche, P. Bøggild, S. Borini, F. H. L. Koppens, V. Palermo, N. Pugno, J. A. Garrido, R. Sordan, A. Bianco, L. Ballerini,

M. Prato, E. Lidorikis, J. Kivioja, C. Marinelli, T. Ryhänen, A. Morpurgo *et al.*, Science and technology roadmap for graphene, related two-dimensional crystals, and hybrid systems, Nanoscale **7**, 4598 (2015).

[3] T. Niu and A. Li, From two-dimensional materials to heterostructures, Prog. Surf. Sci. **90**, 21 (2015).

[4] M. Xu, T. Liang, M. Shi, and H. Chen, Graphene-like two-dimensional materials, Chem. Rev. **113**, 3766 (2013).

[5] A. Nagashima, N. Tejima, Y. Gamou, T. Kawai, and C. Oshima, Electronic Structure of Monolayer Hexagonal Boron Nitride Physisorbed on Metal Surfaces, Phys. Rev. Lett. **75**, 3918 (1995).

[6] A. B. Preobrajenski, S. A. Krasnikov, A. S. Vinogradov, M. L. Ng, T. Käämbre, A. A. Cafolla, and N. Mårtensson, Adsorption-induced gap states of *h*-BN on metal surfaces, Phys. Rev. B **77**, 085421 (2008).

[7] A. B. Preobrajenski, M. A. Nesterov, M. L. Ng, A. S. Vinogradov, and N. Mårtensson, Monolayer h-BN on lattice-mismatched metal surfaces: On the formation of the nanomesh, Chem. Phys. Lett. **446**, 119 (2007).

[8] C. Tan *et al.*, Recent advances in ultrathin two-dimensional nanomaterials, Chem. Rev. **117**, 6225 (2017).

[9] J. J. Jia, T. A. Callcott, E. L. Shirley, J. A. Carlisle, L. J. Terminello, A. Asfaw, D. L. Ederer, F. J. Himpsel, and R. C. C. Perera, Resonant Inelastic X-Ray Scattering in Hexagonal Boron Nitride Observed by Soft-X-Ray Fluorescence Spectroscopy, Phys. Rev. Lett. **76**, 4054 (1996).

[10] H. T. Zhou, J. H. Mao, G. Li, Y. L. Wang, X. L. Feng, S. X. Du, K. Müllen, and H.-J. Gao, Direct imaging of intrinsic molecular orbitals using two-dimensional, epitaxially-grown, nanostructured graphene for study of single molecule and interactions, Appl. Phys. Lett. **99**, 153101 (2011).

[11] S. Berner *et al.*, Boron nitride nanomesh: Functionality from a corrugated monolayer, Angew. Chem., Int. Ed. **46**, 5115 (2007).

[12] K. K. Kim *et al.*, Synthesis of monolayer hexagonal boron nitride on Cu foil using chemical vapor deposition, Nano Lett. **12**, 161 (2011).

[13] R. Y. Tay, M. H. Griep, G. Mallick, S. H. Tsang, R. S. Singh, T. Tumlin, E. H. T. Teo, and S. P. Karna, Growth of large single-crystalline two-dimensional boron nitride hexagons on electropolished copper, Nano Lett. **14**, 839 (2014).

[14] C. Brülke, T. Heepenstrick, N. Humberg, I. Krieger, M. Sokolowski, S. Weiß, F. S. Tautz, and S. Soubatch, Long vertical distance bonding of the hexagonal boron nitride monolayer on the Cu(111) surface, J. Phys. Chem. C **121**, 23964 (2017).

[15] J. Sławińska, I. Zasada, and Z. Klusek, Energy gap tuning in graphene on hexagonal boron nitride bilayer system, Phys. Rev. B **81**, 155433 (2010).

[16] S. Joshi *et al.*, Boron nitride on Cu(111): An electronically corrugated monolayer, Nano Lett. **12**, 5821 (2012).

[17] F. Schulz, R. Drost, S. K. Hämäläinen, and P. Liljeroth, Templated self-assembly and local doping of molecules on epitaxial hexagonal boron nitride, ACS Nano **7**, 11121. (2013).

[18] J. I. Urgel, M. Schwarz, M. Garnica, D. Stassen, D. Bonifazi, D. Ecija, J. V. Barth, and W. Auwärter, Controlling coordination reactions and assembly on a Cu(111) supported boron nitride monolayer, J. Am. Chem. Soc. **137**, 2420 (2015).

[19] C.-A. Palma, S. Joshi, T. Hoh, D. Ecija, J. V. Barth, and W. Auwärter, Two-level spatial modulation of vibronic conductance in conjugated oligophenylenes on boron nitride, Nano Lett. **15**, 2242 (2015).

[20] M. Wang, M. Kim, D. Odkhuu, N. Park, J. Lee, W.-J. Jang, S.-J. Kahng, R. S. Ruoff, Y. J. Song, and S. Lee, Catalytic transparency of hexagonal boron nitride on copper for chemical vapor deposition growth of large-area and high-quality graphene, ACS Nano **8**, 5478 (2014).

[21] S. K. Jang, J. Youn, Y. J. Song, and S. Lee, Synthesis and characterization of hexagonal boron nitride as a gate dielectric, Sci. Rep. **6**, 30449 (2016).

[22] S. K. M. Henze, O. Bauer, T.-L. Lee, M. Sokolowski, and F. S. Tautz, Vertical bonding distances of PTCDA on Au(111) and Ag(111): Relation to the bonding type, Surf. Sci. **601**, 1566 (2007).

[23] O. Bauer, G. Mercurio, M. Willenbockel, W. Reckien, C. H. Schmitz, B. Fiedler, S. Soubatch, T. Bredow, F. S. Tautz, and M. Sokolowski, Role of functional groups in surface bonding of planar π-conjugated molecules, Phys. Rev. B **86**, 235431 (2012).

[24] S. Weiß, I. Krieger, T. Heepenstrick, S. Soubatch, M. Sokolowski, and F. S. Tautz, Determination of the adsorption geometry of PTCDA on the Cu(100) surface, Phys. Rev. B **96**, 075414 (2017).

[25] A. Gerlach, S. Sellner, F. Schreiber, N. Koch, and J. Zegenhagen, Substrate-dependent bonding distances of PTCDA: A comparative x-ray standing-wave study on Cu(111) and Ag(111), Phys. Rev. B **75**, 045401 (2007).

[26] Y. Zou, L. Kilian, A. Schöll, Th. Schmidt, R. Fink, and E. Umbach, Chemical bonding of PTCDA on Ag surfaces and the formation of interface states, Surf. Sci. **600**, 1240 (2006).

[27] S. Duhm, A. Gerlach, I. Salzmann, B. Bröker, R. L. Johnson, F. Schreiber, and N. Koch, PTCDA on Au(111), Ag(111) and Cu(111): Correlation of interface charge transfer to bonding distance, Org. Electron. **9**, 111 (2008).

[28] A. Hauschild, R. Temirov, S. Soubatch, O. Bauer, A. Schöll, B. C. C. Cowie, T.-L. Lee, F. S. Tautz, and M. Sokolowski, Normal-incidence x-ray standing-wave determination of the adsorption geometry of PTCDA on Ag(111): Comparison of the ordered room-temperature and disordered low-temperature phases, Phys. Rev. B **81**, 125432 (2010).

[29] L. Kilian, A. Hauschild, R. Temirov, S. Soubatch, A. Schöll, A. Bendounan, F. Reinert, T.-L. Lee, F. S. Tautz, M. Sokolowski, and E. Umbach, Role of Intermolecular Interactions on the Electronic and Geometric Structure of a Large π-Conjugated Molecule Adsorbed on a Metal Surface, Phys. Rev. Lett. **100**, 136103 (2008).

[30] L. Kilian, E. Umbach, and M. Sokolowski, Molecular beam epitaxy of organic films investigated by high resolution low energy electron diffraction (SPA-LEED): 3,4,9,10-perylenetetracarboxylicacid-dianhydride (PTCDA) on Ag(111), Surf. Sci. **573**, 359 (2004).

[31] T. Ogawa, K. Kuwamoto, S. Isoda, T. Kobayashi, and N. Karl, 3,4:9,10-Perylenetetracarboxylic dianhydride (PTCDA) by electron crystallography, Acta Crystallogr., Sect. B **55**, 123 (1999).

[32] F. S. Tautz, Structure and bonding of large aromatic molecules on noble metal surfaces: The example of PTCDA, Prog. Surf. Sci. **82**, 479 (2007).

[33] M. Rohlfing, R. Temirov, and F. S. Tautz, Adsorption structure and scanning tunneling data of a prototype organic-inorganic

interface: PTCDA on Ag(111), Phys. Rev. B **76**, 115421 (2007).

[34] O. Bauer, Surface bonding of a functionalized aromatic molecule: Adsorption configurations of PTCDA on coinage metal surfaces, Ph.D. thesis, University of Bonn, 2014.

[35] N. Dori, M. Menon, L. Kilian, M. Sokolowski, L. Kronik, and E. Umbach, Valence electronic structure of gas-phase 3,4,9,10-perylene tetracarboxylic acid dianhydride: Experiment and theory, Phys. Rev. B **73**, 195208 (2006).

[36] P. Puschnig *et al.*, Energy ordering of molecular orbitals, J. Phys. Chem. Lett. **8**, 208 (2017).

[37] M. E. Straumanis and L. S. Yu, Lattice parameters, densities, expansion coefficients and perfection of structure of Cu and of Cu-In α phase, Acta Crystallogr., Sect. A **25**, 676 (1969).

[38] C. Wagner, N. Fournier, F. S. Tautz, and R. Temirov, Measurement of the Binding Energies of the Organic-Metal Perylene-Teracarboxylic-Dianhydride/Au(111) Bonds by Molecular Manipulation Using an Atomic Force Microscope, Phys. Rev. Lett. **109**, 076102 (2012).

[39] A. Bondi, van der Waals volumes and radii, J. Phys. Chem. **68**, 441 (1964).

[40] J. Zegenhagen and A. Kazimirov, *The X-Ray Standing Wave Technique - Principles and Applications* (World Scientific, Singapore, 2013).

[41] F. C. Bocquet, G. Mercurio, M. Franke, G. van Straaten, S. Weiß, S. Soubatch, C. Kumpf, and F. S. Tautz, Torricelli: A software to determine atomic spatial distributions from normal incidence x-ray standing wave data, Comput. Phys. Commun. **235**, 502 (2019).

[42] X. Yang, I. Krieger, D. Lüftner, S. Weiß, T. Heepenstrick, M. Hollerer, P. Hurdax, G. Koller, M. Sokolowski, P. Puschnig, M. G. Ramsey, F. S. Tautz, and S. Soubatch, On the decoupling of molecules at metal surfaces, Chem. Commun. **54**, 9039 (2018).

[43] P. Feulner and D. Menzel, Simple ways to improve flash desorption measurements from single-crystal surfaces, J. Vac. Sci. Technol. **17**, 662 (1980).

[44] H. Schlichting and D. Menzel, High resolution, wide range, thermal desorption spectrometry of rare gas layers: sticking, desorption kinetics, layer growth, phase transitions, and exchange processes, Surf. Sci. **272**, 27 (1992).

[45] B. Lehner, M. Hohage, and P. Zeppenfeld, The influence of long-range lateral interactions on the thermodynamics and kinetics of thermal desorption, Chem. Phys. Lett. **379**, 568 (2003).

[46] T. Wagner, H. Karacuban, and R. Möller, Analysis of complex thermal desorption spectra: PTCDA on copper, Surf. Sci. **603**, 482 (2009).

[47] See Supplemental Material at http://link.aps.org/supplemental/10.1103/PhysRevB.99.121404 for the experimental determination of the adsorption energy of PTCDA on hBN/Cu(111).

[48] J. Ikonomov, O. Bauer, and M. Sokolowski, Highly ordered thin films of perylene-3,4,9,10-tetracarboxylic acid dianhydride (PTCDA) on Ag(100), Surf. Sci. **602**, 2061 (2008).

[49] J. Ikonomov, C. H. Schmitz, and M. Sokolowski, Diffusion-limited island decay of PTCDA on Ag(100): Determination of the intermolecular interaction, Phys. Rev. B **81**, 195428 (2010).

[50] M. Schwarz, D. A. Duncan, M. Garnica, J. Ducke, P. S. Deimel, P. K. Thakur, T.-L. Lee, F. Allegretti, and W. Auwärter, Quantitative determination of a model organic/insulator/metal interface structure, Nanoscale **10**, 21971 (2018).

[51] J. Kerfoot, V. V. Korolkov, A. S. Nizovtsev, R. Jones, T. Taniguchi, K. Watanabe, I. Lesanovsky, B. Olmos, N. A. Besley, E. Besley, and P. H. Beton, Substrate-induced shifts and screening in the fluorescence spectra of supramolecular adsorbed organic monolayers, J. Chem. Phys. **149**, 054701 (2018).